Tribology International 171 (2022) 107544

Contents lists available at ScienceDirect

Tribology International

journal homepage: www.elsevier.com/locate/triboint

Electrical compatibility of transmission fluids in electric vehicles

E. Rodríguez [a], N. Rivera [b], A. Fernández-González [c], T. Pérez [d], R. González [b,e], A. Hernández Battez [a,e,*]

[a] Department of Construction and Manufacturing Engineering, University of Oviedo, Pedro Puig Adam, s/n, 33203 Gijón, Spain
[b] Department of Marine Science and Technology, University of Oviedo, Blasco de Garay, s/n, 33203 Gijón, Spain
[c] Department of Physical and Analytical Chemistry, University of Oviedo, Julián Clavería 8, 33006 Oviedo, Spain
[d] REPSOL, C/ Agustín de Betancourt s/n, 28935 Móstoles, Spain
[e] Department of Design and Engineering, Bournemouth University, Poole BH12 5BB, UK

ARTICLE INFO

Keywords:
Electrical conductivity
Transmission fluids
Electric vehicles
Oxidation

ABSTRACT

The in electrical vehicles, where the electric motor is inside the transmissielectrical compatibility of the automatic transmission fluids (ATFs) is very important on and in contact with the ATF. This work studies the influence of factors like temperature, time, and air exposition on the oxidation of three ATFs and their changes in electrical conductivity. The results showed that the higher content of additive the lower variations of electrical conductivity with the oxidation; the measurements of electrical conductivity are better than FT-IR ones for monitoring oil thermo-oxidative degradation at initial periods; the conventional ATFs could maintain good electrical compatibility in electrified drivelines, although their materials compatibility and copper corrosion protection of electrical components should be also tested.

1. Introduction

The electric vehicles (EVs) out-numbered the vehicles propelled by an internal combustion engine (ICE) in the US in the 19st century [1] and the birth of the hybrid electric vehicles (HEVs) took place around 1915 using the ideas included in the US Patent 1.244.025 [2]. The increasing petroleum prices in the 90 ś and tougher environmental regulations led to a serious development of the market of the EVs. In the 21st century, the EVs have gained more attention due to their importance in helping to reduce CO_2 emissions as a requirement of the Kyoto and Paris Protocols on climate change [3,4]. There are four types of electric vehicles: mild hybrid, full hybrid, plug-hybrid and full EV. Such categories have been established taking into account the size of the battery and the electric motors (EMs) used or if the battery is independently chargeable and do not rely on the internal combustion engine (ICE) to generate the electricity [5]. Different configurations of HEVs exist according to the position of the EMs, which could be even inside the transmission and then the transmission fluid will be in contact with the EM.

Most of the EMs used in EVs are switched reluctance motors, alternating current induction motors, and permanent magnet synchronous motors. The heat losses produced in these EMs come from different mechanisms (iron losses, winding losses, magnet losses, mechanical losses, and stray losses) and components (rotor, stator, winding, bearings, etc.) [6]. The rotor and the stator are the most critical temperature locations because the permanent magnet and the winding are in these components, respectively [7]. Recently, the performance and power density of EMs have increased, so the heat generation in the coil due to joule losses has increased [8]. However, in order to avoid demagnetization, the temperature must be below 150 ºC [7]. Thermal modeling of EMs has been used extensively to analyze the cooling performance of EMs and to predict the temperature distribution of the EMs. Both numerical models and lumped parameter thermal network (LPTN) models are commonly used with this purpose [6]. Ponomarev et al. [9] using the Computational Fluid Dynamics (CFD), the thermostatic FEM, and the lumped parameters thermal network (LPTN) models found that the maximum temperature in the copper winding was in the range 130–160 ºC, while the magnet maximum temperature range was 83–110 ºC.

Different options are available for cooling EMs, such as air cooling, liquid cooling (includes oil-cooling), heat conduction enhancement, and hybrid thermal management [6]. Several studies have been conducted on motor cooling with various cooling methods [7]. When using general oil cooling for stator the highest temperature for the rotor was 147 ºC and 104 ºC for the stator [10], while with the oil spray cooling method

* Corresponding author at: Department of Construction and Manufacturing Engineering, University of Oviedo, Pedro Puig Adam, s/n, 33203 Gijón, Spain.
E-mail address: aehernandez@uniovi.es (A.H. Battez).

https://doi.org/10.1016/j.triboint.2022.107544
Received 16 July 2021; Received in revised form 7 March 2022; Accepted 20 March 2022
Available online 23 March 2022

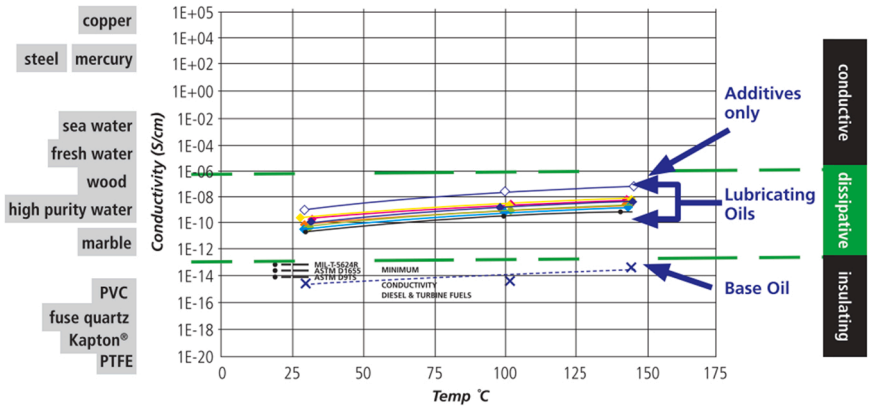

Fig. 1. Electrical conductivity in ATFs [5].

Table 1
Fluid formulation and viscosity of the ATFs.

ATF	Base oils (wt %)	Additive package (wt%)	Kin. visc. ($mm^2 \cdot s^{-1}$)		Viscosity Index
			40 °C	100 °C	
Oil A	Group I (77.7) Group I (10.6)	11.7	39.4	7.7	170
Oil B	Group III (38.3) Group III (50.7)	11.0	29.8	5.8	144
Oil C	Group III (45.0) Group III (38.0)	17.0	36.2	7.4	176

Table 2
Design layout and codes used for oxidation states.

Std. order	Run order	Factorial input variable			Code
		Temp. (°C)	Air flow (L/h)	Aging time (h)	
22	1	170	40	216	8
23	2	170	40	216	8
14	3	150	20	216	5
3	4	150	20	168	1
24	5	170	40	216	8
1	6	150	20	168	1
4	7	170	20	168	3
9	8	150	40	168	2
21	9	150	40	216	6
8	10	150	40	168	2
17	11	170	20	216	7
5	12	170	20	168	3
15	13	150	20	216	5
18	14	170	20	216	7
7	15	150	40	168	2
16	16	170	20	216	7
13	17	150	20	216	5
6	18	170	20	168	3
19	19	150	40	216	6
12	20	170	40	168	4
2	21	150	20	168	1
11	22	170	40	168	4
10	23	170	40	168	4
20	24	150	40	216	6

for coil and housing those temperatures were 107 °C and 89.8 °C, respectively [11]. In addition, with the use of a hybrid cooling method (hollow shaft oil cooling + housing cooling) the temperature of the rotor was 77 °C and the temperature of the stator was 60 °C.

Currently, the lubrication of the electrified vehicles drivelines is carried out mainly by automatic transmission fluids (ATFs), but this solution is not optimized for the performance of the HEVs and EVs [12]. The fact that the ATF can also lubricates the EM demands the compatibility of the oil with the copper in the coils and the polymers used in sensors and seals, an improved thermal conductivity, as well as electrical and magnetic compatibility [12–15]. Regarding electrical compatibility, the electrical conductivity of the oils should be low for avoiding current leaks and possible electric shock and short-circuits in the EM. On the contrary, the oil cannot be an insulator because static buildup followed by static discharges can occur, which could damage equipment [5]. McFadden et al. [16] concluded that the differences in electrical conductivity between different ATFs are small, depend on the amount and type of additives used, and the differences in viscosity have scarce influence. In general, the base oils have very low electrical conductivity and classifies as insulating, while the formulated oils classify as dissipative due to the proper additivation, Fig. 1. Tribology could contribute with different technical solutions to limit the global warming and thus fight against climate change. Among these technical solutions is the formulation of new lubricants [17], which not only reduce both friction and wear, but also fulfill new requirements from systems like the EVs.

The ATFs designed for EVs should maintain the abovementioned properties over time in order to reach a desired fill-for-life. For this reason, the formulation of these fluids should contribute to reduce the oil degradation, which change their properties over time. In addition, the formulators must know how the oil degradation and the parameters that control this process influence on different properties of interest for the EVs. The aim of this work is to study the influence of temperature, time and air flow on the degradation (oxidation) of three commercial ATFs, using as response variable the electrical conductivity of the oil. The Design of Experiment (DoE) technique was used for this analysis and Fourier-transform infrared spectroscopy (FTIR), as usual condition monitoring technique, was also employed.

2. Experimental details

2.1. Transmission fluids

Three commercial ATFs were used in this work. The formulation of these fluids and their kinematic viscosity values at reference temperatures (40 and 100 °C), measured in a Stabinger Viscometer SVM3001, are shown in Table 1.

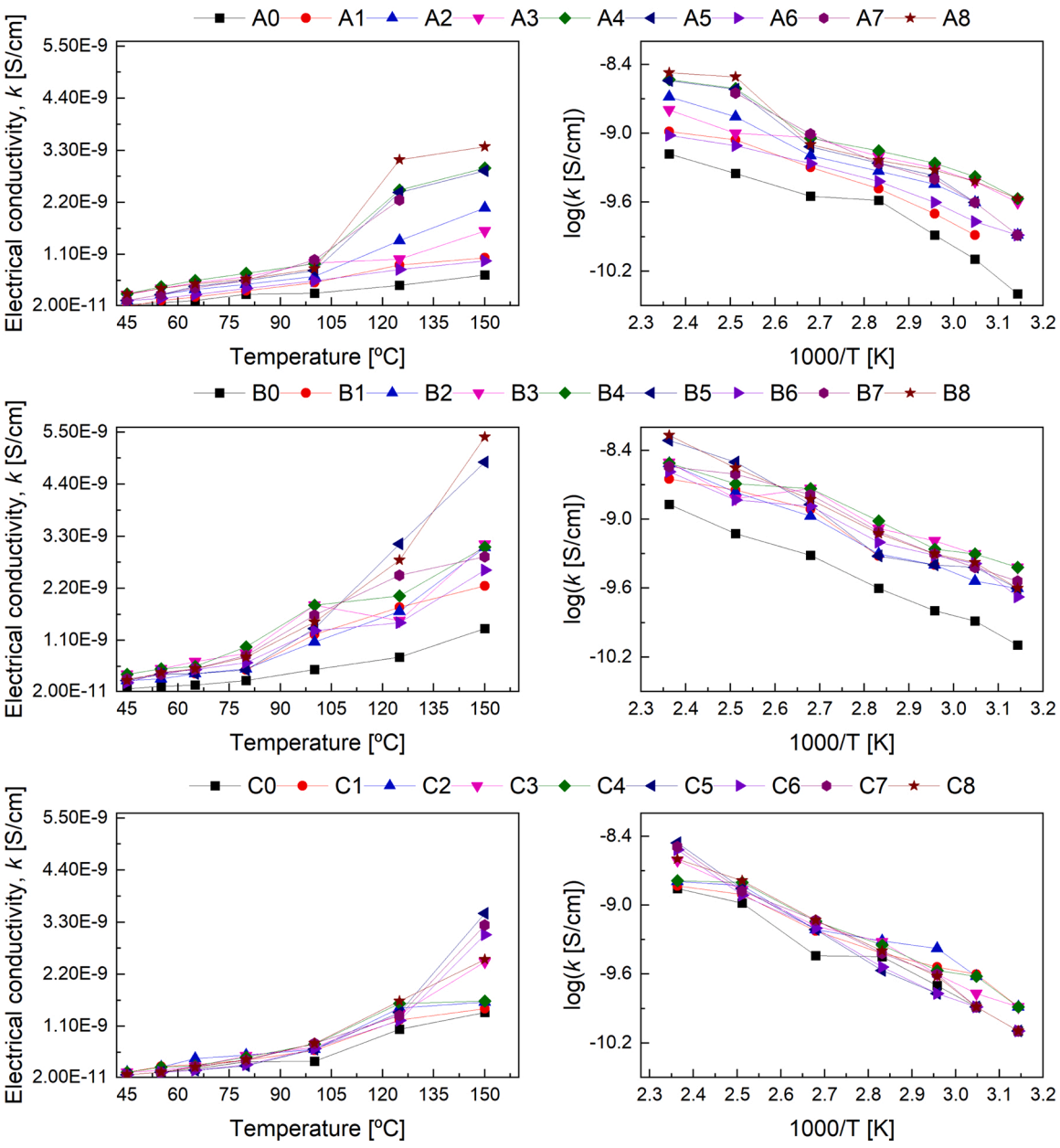

Fig. 2. Electrical conductivity of the fresh (A0, B0 and C0) and aged ATFs.

2.2. Oxidation process, design of experiments and electrical conductivity

The ATFs were aged through an oxidation process controlled by the following parameters: temperature, air flow, and exposure time. The values used for these parameters were: 150 and 170 °C, 20 and 40 L/h, and 168 and 216 h. The influence of these parameters on the oil degradation (oxidation or aging) was analyzed by the design of experiments (DoE) technique using a full-factorial design at two levels (2^3), Table 2. This full-factorial design result in 8 different factors combination, which correspond to different oxidation or degradation states. These oxidation states were coded from 1 to 8.

The response variable used for this DoE analysis was the electrical conductivity at temperatures of 100, 125 and 150 °C. The electrical conductivity of the transmission fluids was measured in the temperature range from 45 to 150 °C by using a Digital Conductivity Meter (Emcee Model 1153). Three electrical conductivity measurements were performed for each `oil sample/temperature/air flow/aging time´ combination. This temperature range was selected taking into account the temperatures reached by the main parts of the EMs during operation, which have been reported in previous works [9–11].

2.3. Viscosity and FT-IR measurements

Among the changes due to the oxidation that can be found in oils are viscosity changes. After the oxidation process conducted, the dynamic viscosity of the ATF samples (fresh and aged) was measured in the range of 20–125 °C in the Stabinger Viscometer SVM3001. The molecular changes occurred in the lubricant samples after the oxidation process were measured by using the Fourier Transform Infrared (FT-IR) Spectroscopy technique. The infrared absorbance spectrum of all lubricant samples was acquired in the range of 4000–600 cm^{-1} at 4 cm^{-1} resolution using a spectrometer Varian 620-IR and a Golden-Gate Attenuated Total Reflectance (ATR) device with a diamond crystal.

The oxidation (or carbonyl oxidation products) of the samples was evaluated by FT-IR determining the peak area taking the absorption band at 1720 cm^{-1}, with a local baseline going through

Table 3
Results of electrical conductivity at 100, 125 and 150 °C.

Run order	Elect. conductivity at 100 °C (pS/cm)			Elect. conductivity at 125 °C (pS/cm)			Elect. conductivity at 150 °C (pS/cm)			Code
	Oil A	Oil B	Oil C	Oil A	Oil B	Oil C	Oil A	Oil B	Oil C	
1	750	1460	710	3090	2630	1630	3380	5220	2500	8
2	830	1500	750	3090	2880	1630	3380	5760	2540	8
3	750	1330	630	2400	3240	1380	2840	4960	3500	5
4	500	1210	630	850	1630	1250	1000	2250	1460	1
5	800	1500	750	3130	2880	1630	3380	5220	2500	8
6	480	1210	580	900	1880	1210	1100	2250	1460	1
7	960	1880	630	1000	1500	1330	1540	3130	2880	3
8	680	1080	630	1380	1630	1500	2080	3090	1580	2
9	520	1250	630	790	1500	1250	1000	2760	3010	6
10	630	1040	580	1420	1880	1500	2100	3100	1630	2
11	980	1630	710	2250	2380	1380	3000	2960	3380	7
12	940	1830	670	1000	1540	1380	1600	3130	2250	3
13	790	1380	630	2400	3100	1400	2880	4880	3480	5
14	980	1630	750	2250	2410	1300	3100	2880	3300	7
15	660	1080	630	1380	1630	1460	2060	3000	1630	2
16	980	1630	750	2250	2410	1300	3040	2760	3040	7
17	800	1330	580	2440	3100	1400	2880	4760	3480	5
18	900	1830	670	1000	1500	1330	1650	3130	2250	3
19	580	1330	630	800	1420	1210	900	2500	3040	6
20	960	1880	710	2460	2130	1580	2880	2960	1630	4
21	540	1250	580	890	1880	1250	1000	2250	1500	1
22	960	1830	750	2460	2130	1580	3000	3130	1640	4
23	880	1830	710	2460	2000	1580	2900	3130	1630	4
24	540	1330	630	750	1500	1210	990	2500	3050	6

Table 4
ANOVA for the electrical conductivity of the oil A at 125 °C.

Source	*df*	*F* value	*p* value	Remark
Model	7	6175.24	< 0.0001	Significant
A - Temperature	1	11,200.18	< 0.0001	
B - Air flow	1	1424.04	< 0.0001	
C - Time	1	7914.84	< 0.0001	
A×B	1	11,787.78	< 0.0001	
A×C	1	947.38	< 0.0001	
B×C	1	7580.84	< 0.0001	
A×B×C	1	2371.60	< 0.0001	
Error	16			
Model summary	R^2	R^2 (adj.)	R^2 (pred.)	Adeq. Precision
	0.9996	0.9995	0.9992	207.81

Table 5
ANOVA for the electrical conductivity of the oil B at 125 °C.

Source	*df*	*F* value	*p* value	Remark
Model	7	116.92	< 0.0001	Significant
A - Temperature	1	17.17	0.0008	
B - Air flow	1	23.91	0.0002	
C - Time	1	283.10	< 0.0001	
A×B	1	287.30	< 0.0001	
A×C	1	9.15	0.0080	
B×C	1	120.61	< 0.0001	
A×B×C	1	77.19	< 0.0001	
Error	16			
Model summary	R^2	R^2 (adj.)	R^2 (pred.)	Adeq. Precision
	0.9808	0.9724	0.9569	29.42

1760–1680 cm^{-1}. The carbonyl-containing degradation products can be esters, aldehydes, lactones, ketones, carboxylate salts, and carboxylic acids. The remaining antioxidant additive (in this case of aminic type) was determined as the peak area at 1515 cm^{-1}, with a local baseline going through 1535–1505 cm^{-1} [18,19].

Table 6
ANOVA for the electrical conductivity of the oil C at 125 °C.

Source	*df*	*F* value	*p* value	Remark
Model	7	115.91	< 0.0001	Significant
A - Temperature	1	188.43	< 0.0001	
B - Air flow	1	242.73	< 0.0001	
C - Time	1	3.75	0.0706	
A×B	1	133.11	< 0.0001	
A×C	1	11.92	0.0033	
B×C	1	78.19	< 0.0001	
A×B×C	1	153.26	< 0.0001	
Error	16			
Model summary	R^2	R^2 (adj.)	R^2 (pred.)	Adeq. Precision
	0.9807	0.9722	0.9565	29.06

3. Results and discussion

3.1. Oxidation process, design of experiments and electrical conductivity

Once obtained the different aged lubricant samples from the three ATFs, the electrical conductivity was measured at different temperatures between 45 and 150 °C, Fig. 2. Considering the electrical conductivity values obtained in the temperature range tested and the different oxidation states, all the lubricant samples can be classified as dissipative ones (electrical conductivity in the range of 10^{-13}-10^{-6} S/cm). The higher differences in electrical conductivity among the fresh sample and the corresponding 8 aged samples were found for the oils A and B, probably due to the lower and similar additive concentration (including antioxidant additive) of these oils in comparison with the oil C. According to the results reported in [5], a difference of one order of magnitude in electrical conductivity is small, but the measurement of this parameter is rapid and effective for condition monitoring of the ATFs over time.

There are numerous factors which explain the increase in electrical conductivity in oils (fresh or aged), but the main reasons are a decrease in viscosity and/or an increase of the oxidation of the oil components (base oil and/or additives) [16]. The electrical conductivity results shown in linear scale and logarithmic scale (Arrhenius plot) in Fig. 2 showed that in general the aged lubricant samples have higher electrical conductivity than the fresh samples. As expected, the electrical

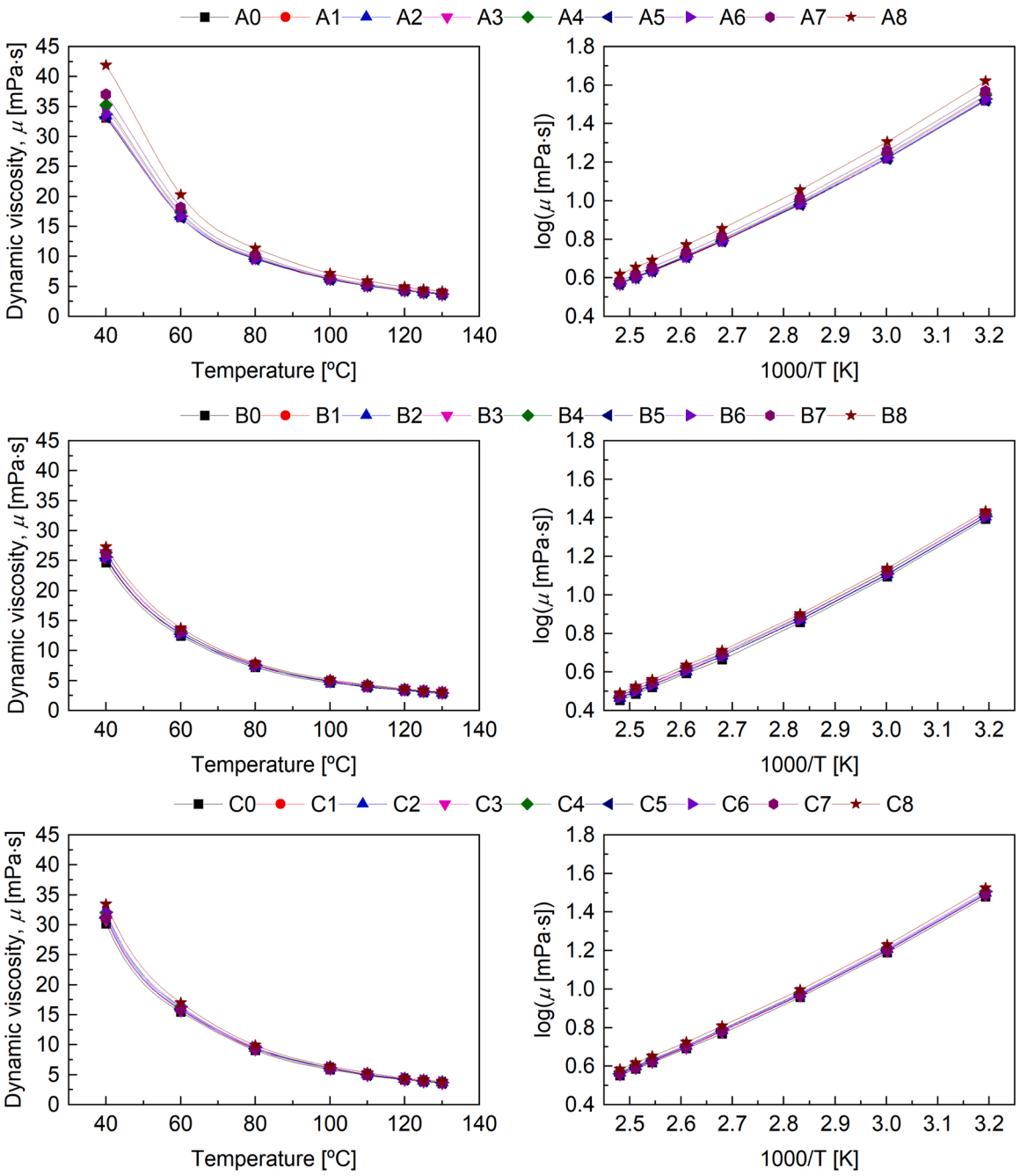

Fig. 3. Dynamic viscosity of the fresh and aged ATFs.

conductivity increased with temperature. This behavior takes place firstly due to the decrease in viscosity, which lead to a rise in ionic mobility and then in electrical conductivity. The ionic mobility in liquids is governed by the Eq. (1) [20].

$$\mu_i = \frac{q}{6\pi\eta r_0} \tag{1}$$

where: μ_i is the ionic mobility, η is the dynamic viscosity, r_0 is the ion radius, and q is the ion charge.

In order to study the influence of temperature, air flow and time on the oxidation of the ATFs and thus on the electrical conductivity. The electrical conductivity at 125 ºC was selected as a measure of the oil oxidation and taken as response variable for conducting an analysis of variance (ANOVA). This temperature was selected as a reference temperature considering the different values reported in [9–11] for the main components in EMs. The results of the measurements of electrical conductivity at 100, 125 and 150 ºC of each oxidized ATF are shown in Table 3. Three replicates of these measurements were included. It is obvious that variations in oil electrical conductivity is a consequence of the aging process and must be related to the physical-chemical changes suffered during the aging. Such changes should be related either with alterations in the viscosity or with chemical transformations through oxidation processes.

The ANOVA was performed using a commercial software of design of experiments (Design-Expert 12) and the effect of the individual factors and their interactions on the oxidation, and how the model fits the experimental data, was proved. The p value< 0.05 means that the model terms are significant within a 95% confidence interval, and the F value determines the effect of each factor, being more significant at larger F values. In addition, the adequate precision, which quantifies the signal-

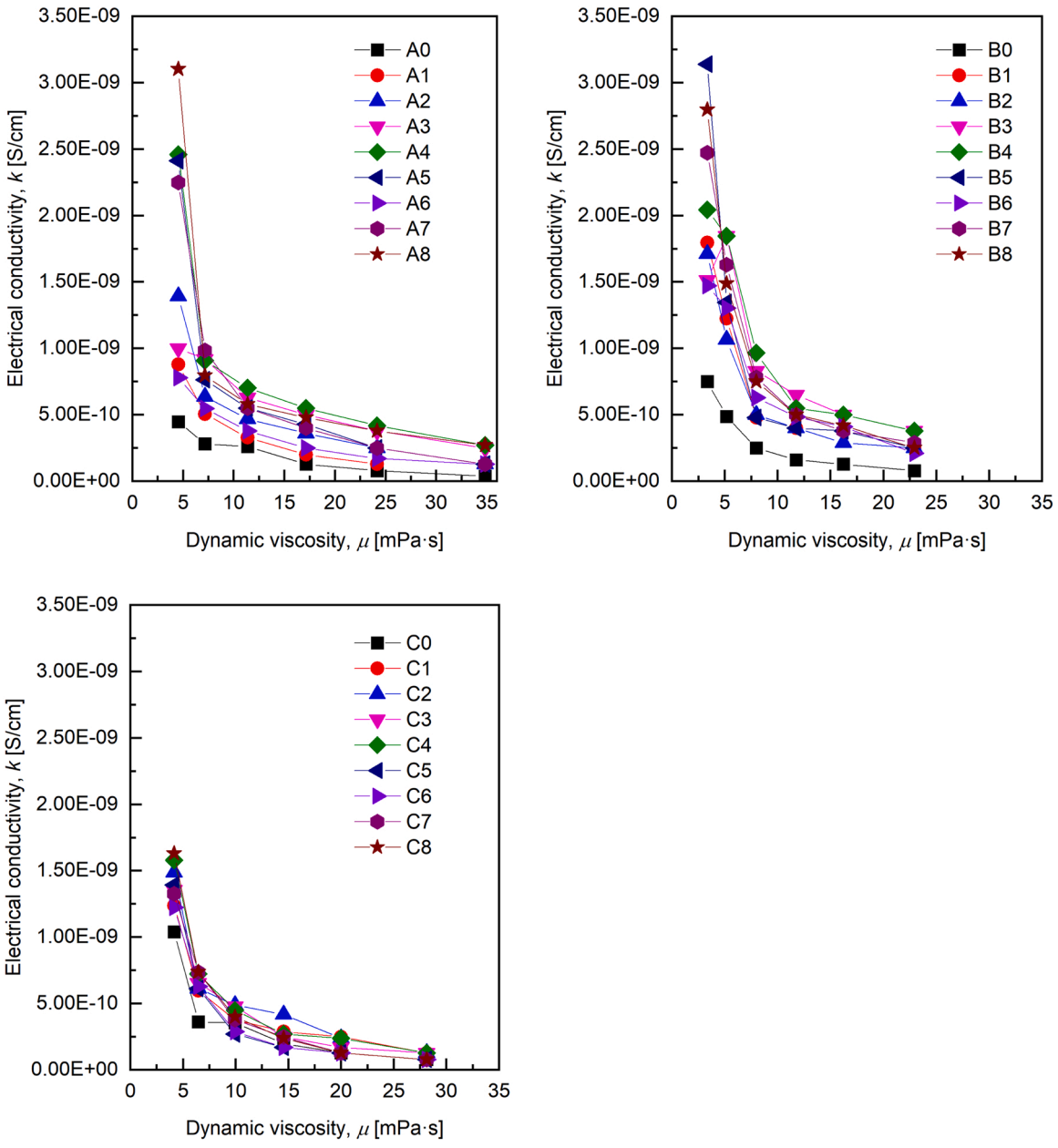

Fig. 4. Electrical conductivity versus dynamic viscosity of the fresh and aged ATFs.

to-noise ratio is desired to be higher than 4, and the lack-of-fit higher than 0.05 also means that the predictive model fit the experimental data very good. Finally, the model was considered statistically precise for R^2 values of 90% or more [21–23].

It can be observed in Table 4 that all the main factors were significant on changes in electrical conductivity of oil A according to its p value. The interactions `temperature × time´, `air flow × time´, and `temperature × air flow × time´ were also significant. The factor with the higher influence on the response was the temperature, followed by the time and the air flow. The regression terms considered significant in the predictive model showed p values lower than 0.05. In this case, the model obtained for the electrical conductivity at 125 °C as a function of the parameters used in the oil aging shows R^2 and R^2 (adj.) values of 0.99, which represent a high accuracy of it. In addition, the signal-to-noise ratio (or adequate precision) was greater to the desired value of 4. These statistical values indicate that the model can predict the response very well within the range of the input variables. The empirical model obtained for the electrical conductivity (expressed in pS/cm) of the oil A is shown as the coded Eq. 1.

$$k = 1785 + 418.33A + 149.17B + 351.67C + 429.17AB + 121.67AC - 344.17BC + 192.50ABC \quad (1)$$

In the case of oil B, all the main factors and their interactions are significant (Table 5). The time was the individual factor with the highest effect on the response, followed by the air flow and temperature. The empirical model obtained has R^2 and R^2 (adj.) values higher than 0.97 and the adequate precision is higher than 4. The coded equation of the empirical model for the electrical conductivity (expressed in pS/cm) is shown as Eq. (2).

$$k = 2115.83 + 83.33A - 98.33B + 338.33C + 340.83AB + 60.83AC - 220.83BC + 176.67ABC \quad (2)$$

For the empirical model of the oil C, according to the p values all the main factors and their interactions were significant with the exception of the time (Table 6). However, the main factor “Time” was included in the

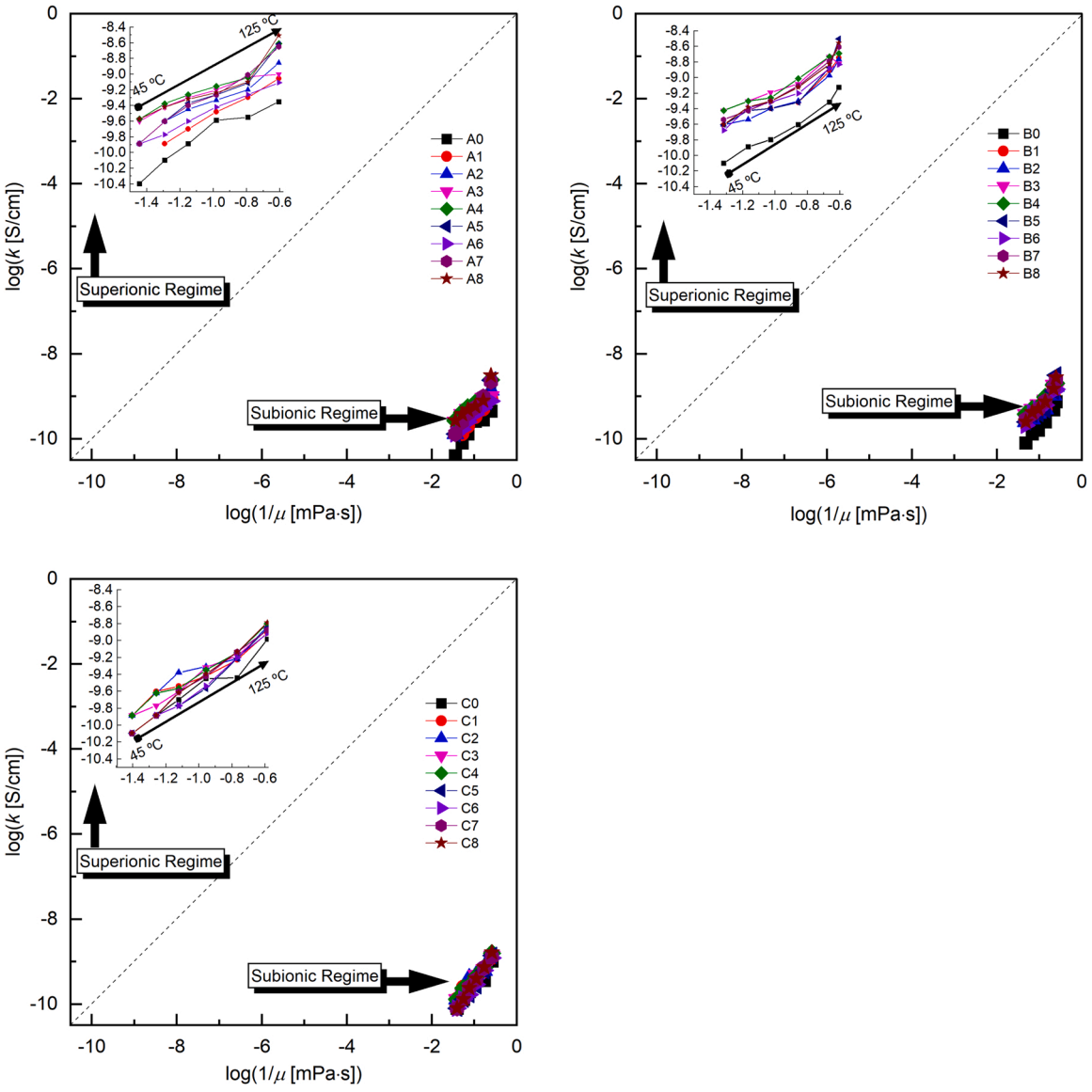

Fig. 5. Walden plot of the fresh and aged lubricant samples.

model because its interactions with the other factors were significant. The model obtained showed R^2 and R^2 (adj.) values higher to 0.97 and an adequate precision greater than 4. The coded equation of this model for the electrical conductivity (expressed in pS/cm) is shown as Eq. (3).

$$k = 1402.92 + 67.92A + 77.08B - 9.58C + 57.08AB + 17.08AC - 43.75BC + 61.25ABC \quad (3)$$

In summary, all the main factors (temperature, air flow and time) are significant, and they influence on the changes in electrical conductivity, so the measurements of this property are a good indicator of the molecular changes in the ATFs due to the oxidation process. In addition, considering the factor coefficients of the coded Eqs. (1)–(3), the relative impact of the factors can be compared. The lower influence of the main factors on the changes in electrical conductivity of the oil C could be attributed to its higher additive content.

3.2. Viscosity and FT-IR

The viscosity versus temperature relationship showed that the viscosity of the aged lubricant samples increased a little compared to the ones of the fresh lubricant samples (Fig. 3), so the variations in electrical conductivity can be associated to the oxidation. This increase was higher at lower temperatures and in the oil A, which was formulated with a mixture of base oils from Group I. These results explain why viscosity is not a parameter for studying the oil chemistry degradation [18]. The increase of viscosity of the aged samples would lead to a decrease in electrical conductivity, but the results shown in Fig. 2 reveal increases in electrical conductivity. Although the increase in electrical conductivity in a maximum of one order of magnitude is not high, the simultaneous increase of viscosity highlights the oxidation occurred in the oil samples. In addition, the viscosity of all the lubricant samples (fresh and aged) was similar at the potential operation temperatures of the ATFs in EVs with the EMs inside the transmission (80–150 °C), but the electrical conductivity was different for similar dynamic viscosity values, Fig. 4. This fact shows the different oxidation states reached with the different thermo-oxidative process used in each lubricant sample.

The Walden plot, representing the log (electrical conductivity) versus log (reciprocal viscosity), was used to evaluate the ionicity of the lubricant samples, Fig. 5. The diagonal dotted line in the Walden plot represents the called “good ionic” liquids. The results obtained show that all lubricant samples are very far from the diagonal in the lower side, so they are considered “non-ionic” liquids. These results are very

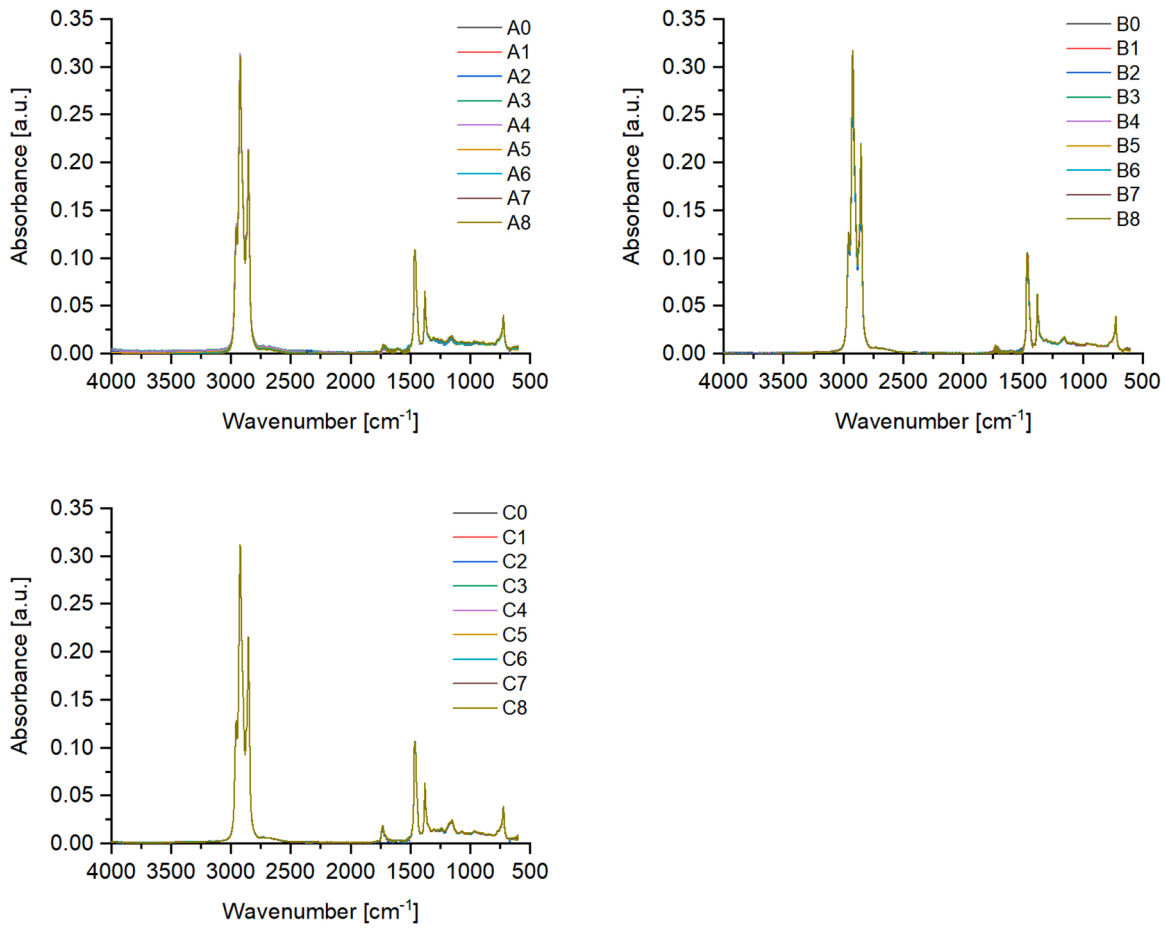

Fig. 6. FT-IR absorbance spectra obtained from the of the fresh and aged ATFs.

important for potential application of these ATFs in an electrified driveline.

Besser et al. [19] described four types of artificial alteration for obtaining degraded oils and one of them (thermo-oxidative alteration at ambient pressure) was used in this work. In addition, three phases were found for all types of artificial alteration: (1) the 'induction phase' consisting in a moderate depletion of the antioxidant additive, which leads to a moderate oxidation increase; (2) the 'antioxidant consumption phase' consisting in a rapid degradation of the antioxidant (AO) additive and a moderate oxidation; and (3) the 'oxidation phase' where a complete depletion of the antioxidant and a very quick increase in oxidation occur.

The FT-IR is a valuable tool for revealing information about oil composition and its degradation and/or contamination. Both oxidation and additive depletion can be detected by this technique, the former through the increase of the corresponding peak because of the formation of organic oxidation products and the latter by the decrease of the corresponding peaks in the spectra [18]. Fig. 6 shows the infrared spectra of all lubricant samples (fresh and aged) and very small changes can be appreciated at first sight.

ATFs are mainly composed of long alkyl chains and, therefore, their FT-IR spectra fits with the expected ones for this kind of compounds. It is clearly seen the characteristic symmetric stretching and asymmetric stretching modes of the ethylene groups from the alkyl chains present at 2853 cm^{-1} and 2920 cm^{-1}, respectively [24], as well as the peaks at 1464 cm^{-1} and 1379 cm^{-1}, both attributable to C–H deformation vibrations of CH_3– aliphatic chains [25]. Changes in absorbance were qualitatively evaluated using the peaks and regions related to the oxidation process and the content of the AO additive (aminic-based) [18], Fig. 7. The ATFs showed an increase in oxidation, which was related to the corresponding antioxidant additive depletion. The oil C had the lower oxidation and antioxidant additive depletion, which could be related to the higher additive content.

The moderate depletion in the antioxidant additive and the moderate oxidation found for all the lubricant samples corresponds to the induction phase of the thermo-oxidative artificial alteration reported by Besser et al. [19]. The evolution of electrical conductivity during the 'AO consumption phase' and the 'oxidation phase' should be determined to correlate the oxidation state with the conductivity values at longer term.

On the other hand, Chimeno-Trinchet et al. [26] evaluated the mid-infrared bands which seems to be correlated to oil aging using artificial neural networks, identifying that absorptions at 2920 cm^{-1}, 889 cm^{-1} and 812 cm^{-1} have the strongest discriminating ability towards the oil aging. However, in the present work the differences in the absorbance at these wavenumbers are nearly undetectable, with differences below 5% of absorbance, suggesting that the aging process followed different pathways.

In order to investigate further into the information gathered by the FT-IR spectra, we performed a Principal Component Analysis of the spectra to check whether the oils clustered somehow. In fact, as shown in Fig. 8, there are four clear different clustering zones: one containing the three fresh oils ('fresh zone'), quite separated from the aged ones; a second one comprising the oils with the mildest aging conditions (samples coded as 1, 'mildest zone'); a third one containing the oil samples coded as 4 and 8 (those with the highest temperature and air flow rate aging conditions, 'F+T+' zone) and a fourth one containing the oil samples aged with the highest air flow rate and the lowest temperature ('F+T–' zone).

Furthermore, the presence of two unexpected points in both 'F+T+' and 'F+T–' zones can be explained taking into account that both of them

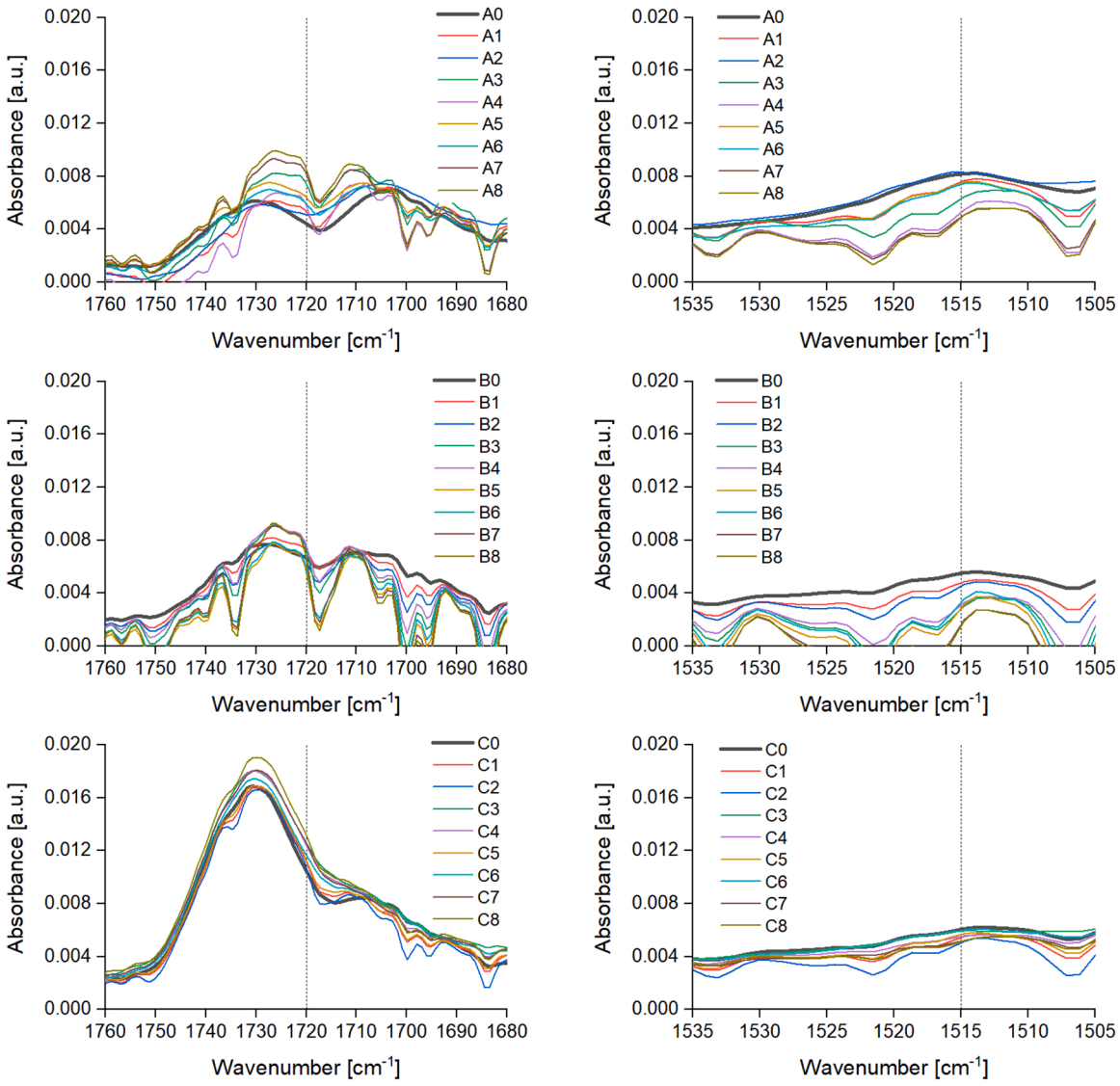

Fig. 7. Spectra regions for oxidation (1760–1680 cm^{-1}) and aminic-based AO additive (1535–1505 cm^{-1}).

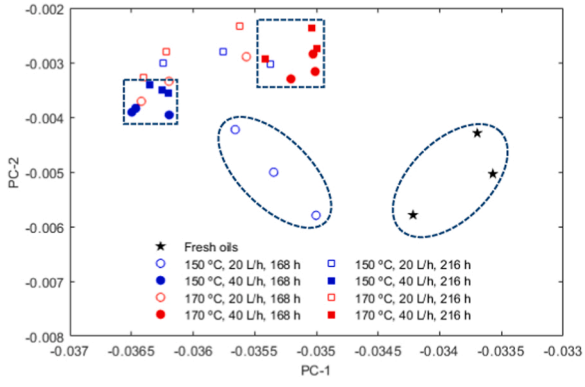

Fig. 8. Principal component representation for all the ATFs (fresh and aged) from the FTIR data.

belong to experiments carried out on oil A, so it is very likely that this situation arises from the very oil nature itself. These experiments allow concluding that the temperature in every case and the air flow rate in the case of oils A and B induce chemical changes in the oils, which are translated into changes in the electrical conductivity.

4. Conclusions

The main conclusions can be draw from the results obtained in this work are:

- The higher content of additive in the oil formulation the lower variations of electrical conductivity with the oxidation.
- The electrical conductivity is a good parameter for monitoring the degradation of ATFs and has greater resolution than FT-IR at initial periods of thermo-oxidative degradation.

- The variation of viscosity was small in the aged ATFs and then the variation in their electrical conductivity was attributed mainly to the oxidation, even at levels not clearly determined by FT-IR.
- All the ATFs (fresh and aged) was grouped under the subionic regime, with increasing electrical conductivity at increasing temperature or decreasing viscosity, but within the range of electrical conductivity classified as dissipative.
- Principal component analysis shows a clear clustering of the oils depending on the aging conditions.
- Additional studies on the electrical conductivity behavior under the *'antioxidant consumption phase'* and the *'oxidation phase'* should be made in the future.

Declaration of Competing Interest

The authors declare that they have no known competing financial interests or personal relationships that could have appeared to influence the work reported in this paper.

Acknowledgments

The authors acknowledge the Ministry of Science, Innovation and Universities (Spain) for supporting the projects under this work was made [grant numbers: PID2019–109367RB-I00 and RTI2018–099756-B-I00].

References

[1] Van Rensselar J. The tribology of electric vehicles. Tribol Lubr Technol 2019;75(1):34–43.
[2] Becker E. Hybrid electric vehicles. Tribol Lubr Technol 2020;76(10):84.
[3] Holmberg K, Erdemir A. The impact of tribology on energy use and CO_2 emission globally and in combustion engine and electric cars. Trib Int 2019;135:389–96. https://doi.org/10.1016/j.triboint.2019.03.024.
[4] Holmberg K, Andersson P, Erdemir A. Global energy consumption due to friction in passenger cars. Trib Int 2012;47:221–34. https://doi.org/10.1016/j.triboint.2011.11.022.
[5] Lubes'n'Greases Perspective on Electric Vehicles Annual Report. LNG Publishing Company, Inc., 2019; 23–27.
[6] Wang X, Li B, Gerada D, et al. A critical review on thermal management technologies for motors in electric cars. Appl Therm Eng 2022;201:117758. https://doi.org/10.1016/j.applthermaleng.2021.117758.
[7] Lee K, Cha H, Kim Y. Development of an interior permanent magnet motor through rotor cooling for electric vehicles. Appl Therm Eng 2016;95:348–56. https://doi.org/10.1016/j.applthermaleng.2015.11.022.
[8] Ha Taewook, Gu Han Nyeon, Soo Kim Min, et al. Experimental study on behavior of coolants, particularly the oil-cooling method, in electric vehicle motors using hairpin winding. Energies 2021;14:956. https://doi.org/10.3390/en14040956.
[9] P. Ponomarev, M. Polikarpova, J. Pyrhönen. Thermal modeling of directly-oil-cooled permanent magnet synchronous machine. Proceedings of 20th International Conference on Electrical Machines, ICEM 2012. 1882–1887. DOI: 10.1109/ICElMach.2012.6350138.
[10] Alexandrova Y, Semken R, Pyrhönen J. Permanent magnet synchronous generator design solution for large direct-drive wind turbines: thermal behavior of the LC DD-PMSG. Appl Therm Eng 2014;65:554–63. https://doi.org/10.1016/j.applthermaleng.2014.01.054.
[11] Lim DH, Lee MY, Lee HS, Kim SH. Performance evaluation of an in-wheel motor cooling system in an electric vehicle/hybrid electric vehicle. Energies 2014;7:961–71. https://doi.org/10.3390/en7020961.
[12] McCoy B. Next generation driveline lubricants for electrified vehicles. Tribol Lubr Technol 2021;77(3):38–40.
[13] Becker E. Gear lubricants in electric vehicles. Tribol Lubr Technol 2021;77(4):80.
[14] Farfan-Cabrera LI. Tribology of electric vehicles: A review of critical components, current state and future improvement trends. Trib Int 2019;138:473–86. https://doi.org/10.1016/j.triboint.2019.06.029.
[15] A. Gangopadhyay, P.D. Hanumalagutti. Challenges and opportunities with lubricants for HEV/EV vehicles. STLE Annual Meeting, 2019. USA.
[16] McFadden C, Hughes K, Raser L, Newcomb T. Electrical conductivity of new and used automatic transmission fluids. SAE Int J Fuels Lubr 2016;9(3):519–26. https://doi.org/10.4271/2016-01-2205.
[17] Holmberg K, Erdemir A. Influence of tribology on global energy consumption, costs and emissions. Friction 2017;5(3):263–84. https://doi.org/10.1007/s40544-017-0183-5.
[18] Dörr N, Agocs A, Besser C, Ristić A, Frauscher M. Engine oils in the field: a comprehensive chemical assessment of engine oil degradation in a passenger car. Tribol Lett 2019;67:68. https://doi.org/10.1007/s11249-019-1182-7.
[19] Besser C, Agocs A, Ronai B, Ristic A, Repka M, Jankes E, et al. Generation of engine oils with defined degree of degradation by means of a large scale artificial alteration method. Tribol Int 2019;132:39–49. https://doi.org/10.1016/j.triboint.2018.12.003.
[20] Abdelmalik AA, Fothergill JC, Dodd SJ. Electrical conduction and dielectric breakdown characteristics of alkyl ester dielectric fluids obtained from Palm Kernel oil. IEEE Trans Dielectr Electr Insul 2012;9(5):1623–32. https://doi.org/10.1109/TDEI.2012.6311509.
[21] Lin Z-C, Ho C-Y. Analysis and application of grey relation and ANOVA in chemical–mechanical polishing process parameters. Int J Adv Manuf Technol 2003;21:10–4. https://doi.org/10.1007/s001700300001.
[22] Zaman PB, Dhar NR. Multi-objective optimization of double-jet MQL system parameters meant for enhancing the turning performance of Ti–6Al–4V alloy. Arab J Sci Eng 2020;45:9505–26. https://doi.org/10.1007/s13369-020-04806-x.
[23] Javidikia M, Sadeghifar M, Songmene V, Jahazi M. Effect of turning environments and parameters on surface integrity of AA6061-T6: experimental analysis, predictive modeling, and multi-criteria optimization. Int J Adv Manuf Technol 2020;110:2669–83. https://doi.org/10.1007/s00170-020-06027-w.
[24] Chimeno-Trinchet C, Pacheco ME, Fernández-González A, Díaz-García ME, Badía-Laíño R. New metal-free nanolubricants based on carbon-dots with outstanding antiwear performance. J Ind Eng Chem 2020;87:152–61. https://doi.org/10.1016/j.jiec.2020.03.032.
[25] Socrates G. Infrared and Raman Characteristic Group Frequencies – Tables and charts. 3rd edition.,. Wiley,; 2001.
[26] Chimeno-Trinchet C, Murru C, Díaz-García ME, Fernández-González A, Badía-Laíño R. Artificial Intelligence and fourier-transform infrared spectroscopy for evaluating water-mediated degradation of lubricant oils. Talanta 2020;219:121312. https://doi.org/10.1016/j.talanta.2020.121312.